

Generalized evolutionary optimum design of fiber-reinforced tire belt structure

J.R. Cho^{*1,2}, J.H. Lee¹, K.W. Kim³ and S.B. Lee¹

¹ School of Mechanical Engineering, Pusan National University, Busan 609-735, Korea

² Research and Development Institute of Midas IT, Gyeonggi 463-400, Korea

³ R&D Center of Kumho Tire Co. Ltd., Gwangju 500-757, Korea

(Received November 04, 2012, Revised August 02, 2013, Accepted October 01, 2013)

Abstract. This paper deals with the multi-objective optimization of tire reinforcement structures such as the tread belt and the carcass path. The multi-objective functions are defined in terms of the discrete-type design variables and approximated by artificial neural network, and the sensitivity analyses of these functions are replaced with the iterative genetic evolution. The multi-objective optimization algorithm introduced in this paper is not only highly CPU-time-efficient but it can also be applicable to other multi-objective optimization problems in which the objective function, the design variables and the constraints are not continuous but discrete. Through the illustrative numerical experiments, the fiber-reinforced tire belt structure is optimally tailored. The proposed multi-objective optimization algorithm is not limited to the tire reinforcement structure, but it can be applicable to the generalized multi-objective structural optimization problems in various engineering applications.

Keywords: fiber-reinforced composite structure; generalized evolutionary optimization; discrete-type multi-objective optimization; genetic algorithm; artificial neural network

1. Introduction

The most significant feature of tire is that the structural and material composition is highly complex, so that the tire performances such as the ride comfort, maneuverability and durability are affected by a number of design variables (Clark 1982). In the early days before the computer-aided simulation and the design technologies had not come into wide use, a new tire model was designed by either the designer's empirical intuition or by the fundamental engineering theories (Purdy 1963). The early studies were mostly limited to the configuration design of tire carcass using quite 2-D simple tire models, targeting for the ride comfort improvement. But since the 1990s, the computer-aided techniques have been extensively employed to model, analyze and design the tire (Lindtner and Tseng 1992, Meschke *et al.* 1995, Danielson *et al.* 1996, Shiraishi *et al.* 2000).

Restricting to the optimum tire design, the most studies focused on either the stiffness distribution of rubber (Abe *et al.* 1996) or the sidewall and crown contours (Nakajima *et al.* 1996, Cho *et al.* 2002, 2005), in order to enhance the wear resistance, durability, ride comfort and maneuverability. In aspect of the objective function, the design problems in the early days were

*Corresponding author, Vice Director, E-mail: jrcho@pusan.ac.kr

mostly single-objective but later multi-objective optimization problems became a main stream. Besides the numerical complexity stemming from the multi-objective optimization, the use of 3-D tire model (Shiraishi *et al.* 2000, Cho *et al.* 2005) significantly increased the size of the tire optimization problem, requiring the extremely long CPU time for the sensitivity analysis invoking the direct finite element analysis. To resolve this difficulty, the evolutionary optimization methods (Huang and Xie 2009, Sarker *et al.* 2002, Gao *et al.* 2012, Brunskill and Lubitz 2012) by utilizing the response surface method, artificial neural network or polynomial functions were adopted to transform the implicit objective function to an explicit approximate one (Nakajima *et al.* 1992, Abe *et al.* 2004).

However, a prominent feature of the tire optimization methods introduced so far is the necessity of the mathematical sensitivity analysis to seek the direction vector of design variables. Regardless of whether the mathematical sensitivity scheme is direct or indirect, the mathematical sensitivity schemes evaluate the gradient of the objective function subject to a set of constraints. Thus, an underlying assumption for conventional tire optimization problems is that the design variables, objective function and the constraints are continuous within the predefined design domain. It implies that conventional sensitivity-driven optimization methods are restricted to improve the initial design models exhibiting a continuous spectral variation in the performances with respect to the continuous design variables and constraints.

The decision of the number of belt layers in the tire tread region becomes an illustrative design problem for which the optimization methods relying on the mathematical sensitivity analysis encounter the difficulty in seeking an optimum solution. This kind of situation may, but frequently, occur when the designer tries to improve the target performances by introducing a new design model which is different from the initial one in aspects of the structural or/and material composition. A distinct characteristic of this kind of optimization problems is that the design variables change in the discrete manner, so that the continuous spectral variation of the objective functions to the design variables does not secure any more. In short, in this kind of discrete-type optimization problems, neither the objective function gradient is defined nor the mathematical sensitivity to the design variables is derivable.

An alternative way to avoid the mathematical sensitivity analysis is to adopt the evolution of a number of design model candidates using genetic algorithm (Holland 1975, Goldberg 1989, Gao *et al.* 2012). As is well known, in the optimum design using genetic algorithm a best design model is chosen through the iterative genetic evolution composed of the fitness test, reproduction, crossover and mutation operations. As a result, both the sensitivity analysis and the direction vector which are essential for the conventional sensitivity-driven optimizations are completely unnecessary. Since the theoretical framework for genetic algorithm was laid down by Holland (1975), genetic algorithm has been rapidly spread to a variety of optimization problems in science and engineering fields (Govindaraj and Ramasamy 2005, Kameshki and Saka 2007, Rahami *et al.* 2008). But, the employment of genetic algorithm for the tire optimization was somewhat lately started from the late of 1990s. To the best of our literature survey, Hoffmeister and Bernard (1998) applied genetic algorithm to the optimum arrangement of tread pitch and Abe *et al.* (2004) used genetic algorithm to optimally design the fiber-reinforced belt layer.

In this context, this paper addresses a generalized multi-objective optimization of fiber-reinforced belt layer of automobile tire by making use of genetic algorithm and artificial neural network to simultaneously enhance the cornering performance and the durability. Here, the term *generalized* indicates that the proposed method is not subject to the types of design variable and objective function, even though only two specific numerical examples are presented in this paper.

In the multi-objective optimization of the fiber-reinforced belt layer, the fitness of each design model is evaluated with the help of the surrogate models of individual single-objective functions which are approximated by artificial neural network. In the current study, we present a number of Pareto solutions for different weighting factors, instead of seeking a best Pareto solution by trading-off the aspiration levels (Nakayama and Furukawa 1985). But, the seeking of a best Pareto solution using the proposed method is straightforward when the aspiration levels of each objective function are adjusted by the procedure introduced in our previous paper (Cho *et al.* 2002).

2. Discrete-type tire structure design

Referring to Fig. 1, tire is composed of a number of components which can be broadly classified into the pure rubber parts and the fiber-reinforced (FRR) parts. Here, the fiber-reinforced parts are belt layers in the tread region, polyester-cord layer called carcass and steel cords in the bead region. Besides forming the underlying skeleton of tire, these reinforcement components play an important role in the static and dynamic performances of tire, such as the ground contact, wear, durability, ride comfort and rim fitting. For this reason, these components have been importantly considered in the tire design, for which the specific design methods have been introduced by many investigators, from the earlier empirical and theoretical methods (Purdy 1963, Clark 1982) to the recent FEM-utilized mathematical optimization techniques. One of the significant features of the traditional optimum design of the tire structures design is that most concerns focused on the carcass contour in the sidewall, tread or bead regions. Regarding other design variables like the number of layers and cords and the belt angle and width, the decision making was mostly made based upon the parametric investigation of the target performance to these design variables (Satamurthy and Hirschfeldt 1987).

In the conventional optimum tire design, the change in geometry coordinates of the initial tire design does not remarkably change the finite element mesh. It is because not only the geometry change is not large but all the finite elements in the vicinity of the design object like the carcass layer move simultaneously during the mesh adaptation for the iterative sensitivity analysis (Nakajima *et al.* 1996, Cho *et al.* 2002). But, in the tire structure optimization in which the

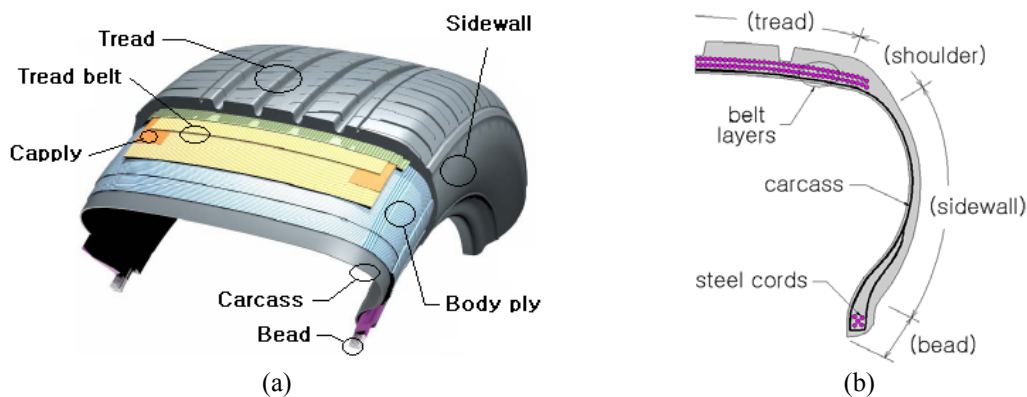


Fig. 1 Radial pneumatic tire: (a) composition; (b) major reinforcement components

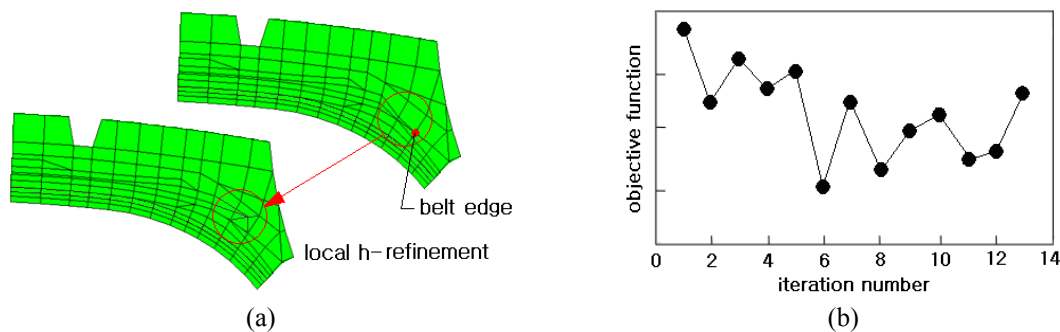


Fig. 2 Representation: (a) local h -refinement; (b) instability of objective function

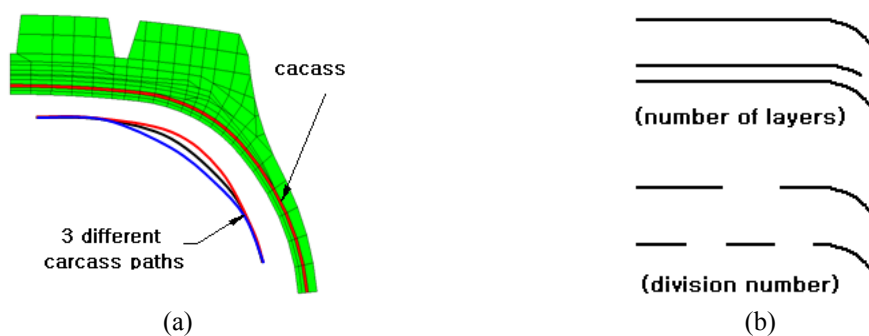


Fig. 3 Discrete-type design variable: (a) carcass path; (b) fiber-reinforced belt layer

configuration and dimensions of the design object change significantly as illustrated in Fig. 2(a), the uniformity of the initial finite element mesh may be significantly deteriorated. Being non-uniformity of finite element mesh during the mesh adaptation for the iterative sensitivity analysis inevitably causes the excessive fluctuation of the objective function to the optimization iteration number, as shown in Fig. 2(b). As a result, one may encounter the numerical difficulty in reaching a converged optimum solution, unless the local h -refinement (Demkowicz *et al.* 1989, Cho and Park 2003) is employed to recover the mesh uniformity. This kind of the fluctuation of objective function is different from the inherent fluctuation of objective function owing to the change of design variables in the iterative optimization process.

Meanwhile, the design variables in the tire design may change in the discrete manner, which may frequently happen when the designer tries to generate a new tire model by greatly modifying the existing design model. As depicted in Fig. 3, the carcass path, the total number and the division number of belt layers could be the representative examples of the discrete-type design variables. This kind of tire structure design has never done before by the mathematical optimization method, rather it was made based on either the bench mark test or the parametric numerical analysis. It is because the gradient of objective function to the design variables is not mathematically defined as mentioned earlier, which became a main motivation that genetic algorithm has been introduced to the tire structure design. Not being confined to the discrete-type optimization problems, genetic algorithm would also be applied to the conventional optimum design in which the design variables and objective function vary continuously. Furthermore, the CPU time required for the fitness test

of each genome during the iterative genetic evolution can be greatly reduced if the direct finite element analysis is replaced with the surrogate models (Simpson 1991, Cho *et al.* 2011, Gao *et al.* 2012), particularly for the large-scale optimization problems.

3. Generalized evolutionary multi-objective structure optimization

3.1 Formulation of discrete-type multi-objective optimization

In this section, we consider the generalized multi-objective optimization problems characterized by distinct discrete-type design variables. According to the type of design variables, a design variable vector X consisted of the total of nd design variables is divided into a number of distinct design variable vectors X_I ($I = 1, 2, \dots, ng$) such that

$$X = X_1 \oplus X_2 \oplus \dots \oplus X_{ng} = \{X_1, X_2, \dots, X_{ng}\}^T, \quad ng \leq nd \quad (1)$$

$$X_I = \{X_1, X_2, \dots\}_I^T \quad (2)$$

Note that ng becomes identical to nd when all the distinct design variable vectors X_I include only one design variable. In the similar manner, a multi-objective function $F(X)$ is composed of a finite number of single-objective functions $f_i(X)$ ($i = 1, 2, \dots, no$),

$$F(X) = \{f_1(X), f_2(X), \dots, f_{no}(X)\} \quad (3)$$

subject to a set of inequality and equality constraints given by

$$g_j(X) \leq 0, \quad j = 1, 2, \dots, m \quad (4)$$

$$g_j(X) = 0, \quad j = m + 1, \dots, nc \quad (5)$$

Hereafter, we denote the quantities $(\cdot)^k$ be those at the k -th trade-off stage in an iterative multi-objective optimization process. Referring to the satisficing trade-off method (STOM) introduced by Nakayama and Furukawa (1985) and Cho *et al.* (2002), we employ the concept of the ideal and aspiration levels of each single-objective function $f_i(X)$ is introduced to define a weighted multi-objective function $F^k(X)$ at the k -th trade-off stage

$$F^k(X) = \max_{1 \leq i \leq no} \left\{ w_i^k \left| f_i^* - f_i(X) \right| \right\}, \quad w_i^k = \left| f_i^* - \hat{f}_i^k \right|^{-1} \quad (6)$$

The ideal levels f_i^* indicate the highest values which f_i are expected to be reached, while the aspiration levels \hat{f}_i^k are the desired values to be improved from the current values. In general, the former levels are determined by the single-objective optimization while the latter levels are set by the designer. The weighting factors w_i are to be automatically set once these two levels are given.

Next, the weighted multi-objective function $F^k(X)$ subject to the constraints is transformed to an unconstrained pseudo-objective function $U^k(X, r_p)$ given by

$$U^k(X, r_p) = F^k(X) + r_p \sum_{j=1}^{nc} \max [0, c_j^k g_j(X)]^2 \quad (7)$$

with a penalty parameter r_p . The factors c_i for scaling the magnitudes of each constraint with respect to the magnitude of the weighted multi-objective function $F(X)$ are calculated through

$$c_j^k = |F^k(X)| / |g_j(X)| \quad (8)$$

Letting X_i be the discrete-type design variables governing the tire reinforcement structure and $f_i(X)$ be the tire performances evaluated by the tire static contact analysis, the multi-objective optimization of the tire reinforcement structure is formulated as follows

$$\text{Minimize}_X \quad U^k(X, r_p) \quad (9)$$

$$\text{Subject to:} \quad \int_{\Omega^{k,0}} S_{ij}(\mathbf{u}) e_{ij}(\mathbf{v}) dV = \int_{\Omega^{0,k}} \rho^0 b_i^k dV + \int_{\partial\Omega_N^{0,k}} \hat{t}_i^0 v_i ds \quad (10)$$

$$g_j(\mathbf{X}) \leq 0, \quad 0 \leq j \leq m \quad (11)$$

$$g_j(\mathbf{X}) = 0, \quad m+1 < j \leq nc \quad (12)$$

with $\Omega^{k,0}$, $\partial\Omega_N^{k,0}$ and b_i^k being the initial material domain, the traction boundary region and the body force of the k -th discrete tire structure model. And, \hat{t}_i^0 is the traction force converted to the initial tire configuration and $S_{ij}(u)$ and $e_{ij}(v)$ are the Second Piola-Kirchhoff stresses and the green-Lagrange strains, respectively. Note that Eq. (10) stands for the total Lagrangian formulation of the tire static contact problem (Bathe 1996, Cho *et al.* 2005).

A best Pareto solution of the problem Eq. (9) is to be sought through the iterative trade-off process in which each trade-off involves the inner loop of iterative genetic evolution. All the single-objective functions f_i are approximated using artificial neural network, and all the ideal levels f_i^* are chosen by the single-objective optimization utilizing genetic. The sensitivity analysis required for the inner iteration loop is replaced with the iterative genetic evolution process.

3.2 Genetic algorithm

Once an initial population of genomes is generated, a genetic evolution of the genome population undergoes a series of fitness test, selection, crossover and mutation in sequence (Holland 1975, Goldberg 1989). And, the genome ranked top among all the genomes which are survived through a number of genetic evolutions is taken as a best one. In order to apply genetic algorithm to an engineering optimization problem, each design model $M_{ID} = \{X_1, X_2, \dots, X_{nd}\}_{ID}^T$ under consideration should be transformed to genomes G_{ID} which are expressed by the total number of m_{nd} bits. Here, $m_{nd} \in \mathfrak{R}^+$ is determined from the relation of $2^{m_{nd}} \geq N_{TOT}^{case}$ with N_{TOT}^{case} calculated by

$$N_{TOT}^{case} = N_1^{case} \times N_2^{case} \times \dots \times N_{nd}^{case} \quad (13)$$

when N_i^{case} is denoted as the case number of the i -th design variable. For the current study, the

genome G_{ID} corresponding to the ID -th discrete-type tire structure model M_{ID} in the following binary form

$$G_{ID} = b_1 b_2 \cdots b_{m_1} \cdots b_{m_{(j-1)}} \cdots b_{m_j} \cdots b_{m_{nd}}, \quad ID = 1, 2, \dots, N_{pop} \quad (14)$$

where b_i are either 1 or 0 and $b_{m_{(j-1)}} \cdots b_{m_j}$ stands for the j -th design variable X_j . Then, an initial population \mathcal{G}_G^0 of N_{pop} genomes is defined by

$$\mathcal{G}_G^0 = \{G_{ID}^0 : ID = 1, 2, \dots, N_{pop}\} \quad (15)$$

On the other hand, the decoding of a binary string to transform genomes G_{ID} to corresponding discrete-type tire structure models $M_{ID} = \{X_1, X_2, \dots, X_{nd}\}_{ID}^T$ is carried out string-interval-wise. For example, once a string interval $b_{m_{(j-1)}} \cdots b_{m_j}$ is mapped into a decimal number, then this decimal number indicates the specific one among the total of N_j^{case} number of X_j .

The initial population of genomes is generated randomly so that the selection of genomes having high fitness is needed to seek a best genome in the minimum number of genetic evolutions. The selection process is made based on the fitness test of each genome in the population, and it prepares parents to reproduce offsprings through the crossover and mutation operations. Both the fitness test and the selection operation are carried out after an initial genome population is generated and after every mutation operation in the iterative genetic evolution process. Several methods such as roulette-wheel, tournament, ranking and sharing have been introduced for the genome selection operation (Kameshki and Saka 2007), but the roulette-wheel selection method is adopted for the current study. The fitness of each genome G_{ID} at the ℓ -th genetic evolution stage is calculated using the fitness function defined by

$$U^{k,\ell}(G_{ID}, r_p) = F^{k,\ell}(G_{ID}) + r_p \sum_{j=1}^{nc} \max[0, c_j^{k,\ell} g_j(G_{ID})]^2, \quad \ell = 1, 2, \dots \quad (16)$$

where the superscript k stands for the iteration number of trade-off between the single-objective functions $f_i(G_{ID})$. As a convergence criterion to terminate the iterative genetic evolution, we use the maximum repetition times N_{GA}^{con} of successive generations with the best fitness value unchanged. Meanwhile, the genetic evolution is forced to iterate up to the preset minimum generation number N_{GA}^{for} without the fitness test at the initial stages, in order to rule out any pre-converged unsatisfactory solution.

Once the parent genomes are prepared through the fitness test and the selection job, the offspring genomes are reproduced through crossover and mutation in sequence. Crossover and mutation are performed in order to extend the search space of genomes, which may produce more excellent offspring genomes with higher fitness. In proportion to the crossover and mutation ratios, the search space becomes larger but the convergence speed becomes lower, so the crossover and mutation ratios are usually set by 80~95% and 0.1~1.0% respectively. For the current study, we employ the one-point crossover operator and the classical mutation operator (Smith and Holland 1987).

3.3 MOGA optimization algorithm

Flowchart of a multi-objective genetic algorithm (MOGA) optimization method is represented

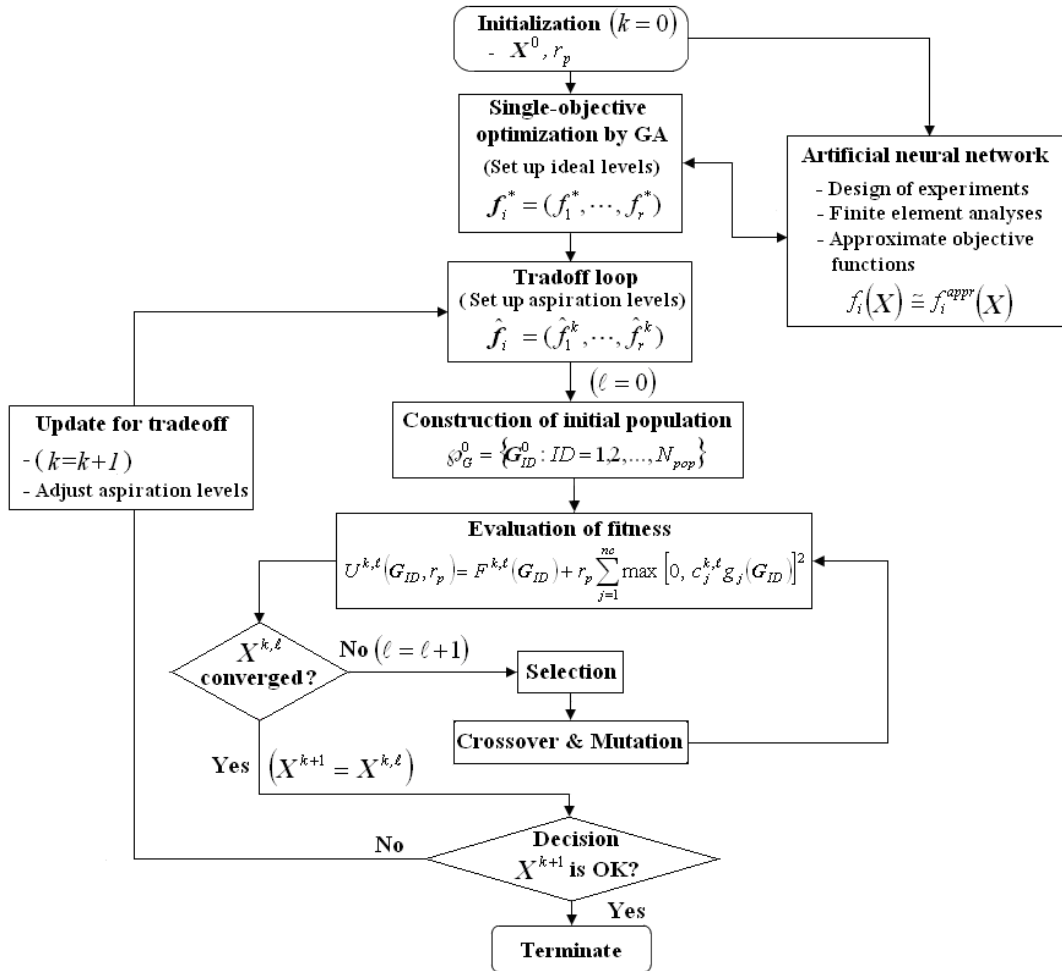


Fig. 5 Flowchart of MOGA optimization method

in Fig. 5, where trade-off, genetic algorithm and artificial neural network are combined. This method is basically composed of two main iteration loops, the outer loop for the trade-off between the single-objective functions and the inner loop for the genetic evolution of genomes. Individual single-objective functions $f_i(G_{ID})$ approximated by artificial neural network are used for the single-objective optimization and the fitness test, and the single- and multi-objective optimizations are carried out by genetic algorithm. The inner loop terminates when the preset convergence criterion is satisfied, while the outer loop is terminated by the designer's own judgment.

The MOGA optimization starts with the initial design variables X^0 and a penalty parameter r_p after each single-objective function is approximated by artificial neural network. Next, the ideal levels for each single-objective functions are chosen with the help of the single-objective optimization and the initial aspiration levels are set by the designer. With the initial setting of the aspiration levels \hat{f}_i , an optimum solution is sought through the iterative genetic evolution composed of fitness test, selection, crossover and mutation. The optimum solution $X^{k,\ell}$ satisfying

the convergence criterion set for genetic algorithm is satisfactory then the optimization process is completely terminated, otherwise the trade-off iteration repeats with the modified aspiration levels. The reader may refer to Nakayama and Furukawa (1985) for more details on the trade-off process between single-objective functions.

Referring to our previous paper (Cho *et al.* 2005), an artificial neural network with two hidden layers and the sigmoid transfer function $f(x) = 1 / (1 + e^{-x})$ is employed. And the design of experiments (DOE) is prepared by an orthogonal array $L_{3^m} (3^{(3^m-1)/2})$, where the level of design variables is set by three. The target output data f_i^{TAR} of individual single-objective functions to the input design variables X^{INP} in DOE are prepared by the finite element analysis. The weighting factors w_{ij} connecting the input, hidden and output layers are iteratively computed through a series of the forward computing and the backward learning. The iteration for determining the weighting factors terminates when the output signals f_i^{OUT} satisfy the convergence criterion defined by

$$\max_{s,i} \left| \frac{f_{i,s}^{OUT} - f_{i,s}^{TAR}}{f_{i,s}^{TAR}} \right| \leq \varepsilon_{ANN}, \quad i = 1, 2, \dots, no, s = 1, 2, \dots, N_{DOE} \quad (17)$$

where no and N_{DOE} denote the number of individual single-objective functions $f_i(X)$ and the experiment cases in *DOE*, respectively.

4. Numerical experiments

A test multi-objective optimization program called MOGA(multi-objective genetic algorithm) program is coded according to the theoretical formulae described in Section 3. The finite element analyses required to learn artificial neural network are performed by ABAQUS/Standard (2002). The structure of tread belt of an automobile tire mode P225/55R16 shown in Fig. 6(a) is desired to be tailored to simultaneously improve the durability and the cornering coefficient (CC). This tire model is composed of a single carcass layer, two tread belt layers and two capply layers with the geometry and material properties given in Table A1 in appendix. The hyperelastic rubber components are modeled using a two-term linear Moonley-Rivlin model and the detailed properties may be referred to our previous paper (2005). The tire durability is mostly influenced by the peak strain energy in the shoulder region as depicted in Fig. 6(b), so the peak strain energy in this region is taken as a single-objective function. Fig. 6(b) is cut from the tire part which is in contact with the ground, and note that the finite element analysis was carried out with 3-D full tire model shown in Fig. 6(a). While the tire cornering coefficient is defined by the ratio of the lateral force to the vertical force acting on the tire, and it is determined once the lateral force is obtained by finite element analysis.

The 3-D finite element model shown in Fig. 6(a) is constructed by considering only the main grooves and the tire model is non-uniformly discretized with the total of 28,800 C3D6H and C3D8H elements provided by ABAQUS. Two tread belt layers and a carcass layer embedded in the underlying rubber matrix are modeled using rebar elements, and steel cords and underlying rubber matrix in the bead region are modeled as homogenized solid elements based on the linear rule of mixture. The tire axis and the outer bead nodes being in contact with the tire rim are connected using a number of massless rigid elements, and the tire axis is constrained to be clamped. The ground is modeled as a rigid plate and the vertical load F_y of 495 kgf is applied to the tire bottom surface by moving up the rigid plate. The tire model is inflated up to the internal

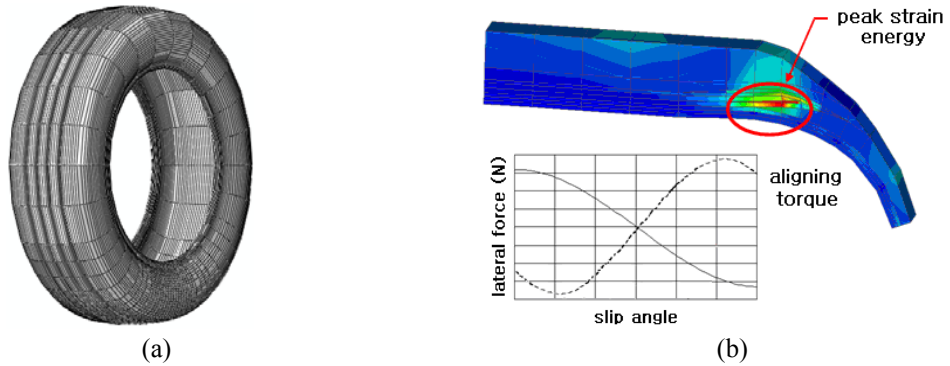


Fig. 6 Design model: (a) finite element mesh; (b) peak strain energy and cornering coefficient (CC)

pressure p of 30 psi, and the friction coefficient μ between the tire and the ground is set by 1.0.

As shown in Fig. 7, there exist two belt layers in the tread region and two types of design variables, the belt angle X_1 and the belt width increment X_2 , constitute a design variable vector $X = X_1 \oplus X_2$. Here, X_1 is composed of angles θ_1 and θ_2 of belt #1 and #2 while X_2 consists of the belt width increments Δb_1 and Δb_2 of belt #1 and #2. As a result, the total number of design variables contained in the design variable vector X is as follows: $nd = 2 + 2 = 4$. These two types of design variables are subjected to the constraints given by $21^\circ \leq X_1 \leq 27^\circ$ and $-10 \text{ mm} \leq X_2 \leq +10 \text{ mm}$ respectively, so that the case numbers of each design variable are $N_1^{case} = N_2^{case} = 61$ and $N_3^{case} = N_4^{case} = 201$. Using the relation of $2^{nd} \geq N_{TOT}^{case}$ in Section 3.2.1, a binary string must have 27 bits to express each design variable vector X . In order to approximate the two single-objective functions $f_i(X)$ by artificial neural network, 9 cases of finite element analyses are carried out according to the $L_9(3^4)$ orthogonal array DOE. Three levels set for the belt angle and the belt width increment are $(21^\circ, 24^\circ, 27^\circ)$ and $(-10 \text{ mm}, 0, +10 \text{ mm})$ respectively, and the convergence tolerance ϵ_{ANN} is set by 0.01.

The simulation parameters taken for genetic algorithm are as follows: N_{pop} of 50, the crossover ratio of 0.8, the mutation ratio of 0.01, N_{GA}^{for} of 30, and N_{GA}^{con} of 7, respectively. It was observed through the preliminary experiments that the total number of genetic evolutions required to obtain a converged genome increases in proportion to N_{pop} , the crossover and mutation ratios and N_{GA}^{con} .

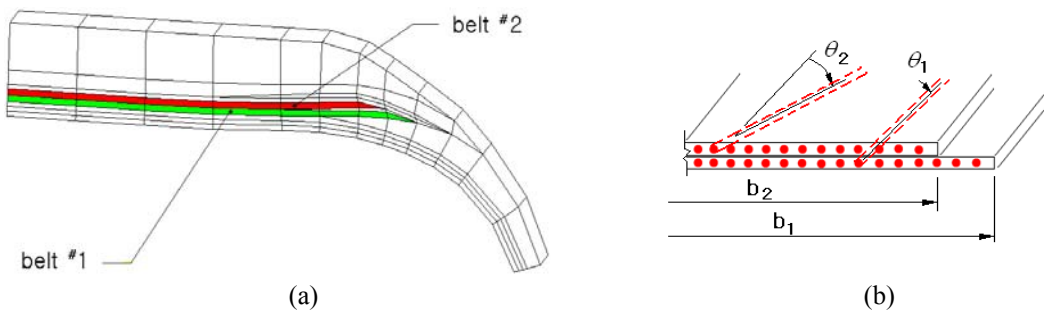


Fig. 7 Design variables for the optimum design of fiber-reinforced belt layer

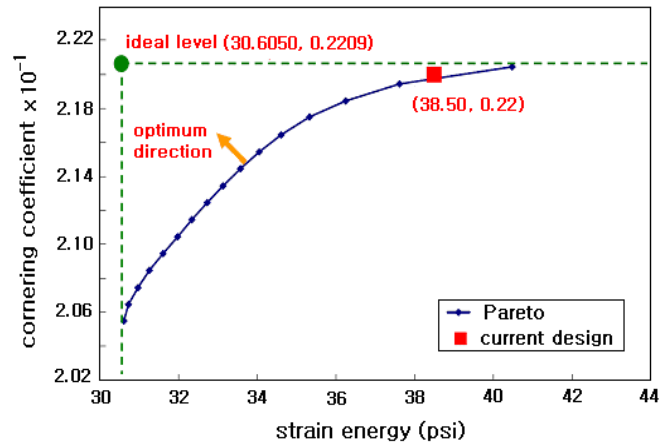


Fig. 8 Pareto curve for the fiber-reinforced belt layer

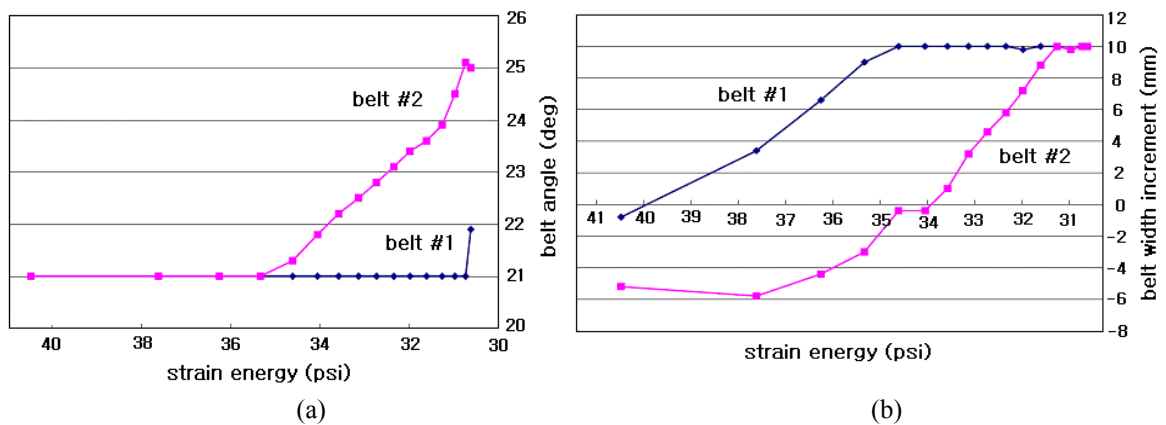


Fig. 9 Sensitivity of the peak strain energy: (a) to the belt angle, (b) to the belt width increment

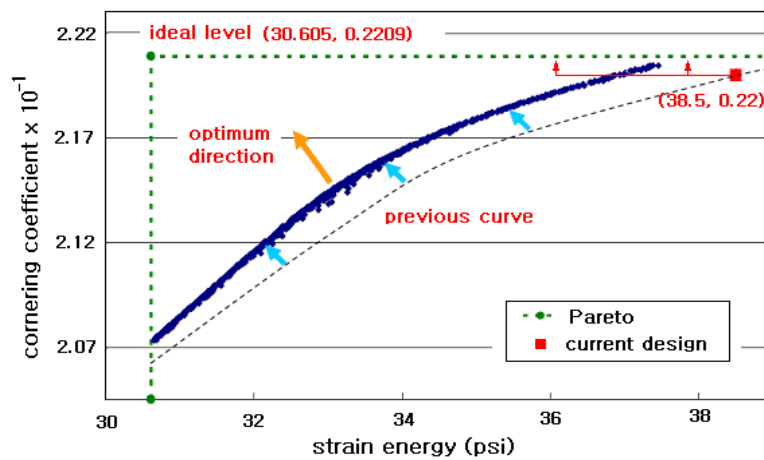


Fig. 10 Pareto curve for the adjusted constraints

Table 1 Multi-objective optimization results when the constraints are extended

Aspiration-level adjustment	Objective functions		Optimum design variables			
	Peak strain Energy (psi)	Cornering coefficient	Belt angles (deg)		Width increments (mm)	
			#1	#2	#1	#2
1	36.9342	0.22001	19.0	19.0	+11.4	-6.9
2	36.9903	0.22001	19.0	19.2	+9.3	-9.9
3	37.0115	0.22010	19.2	19.2	+10.2	-9.4
4	37.0303	0.22008	19.0	19.0	+10.2	-7.5
5	37.0541	0.22013	19.0	19.4	+10.8	-7.8
6	37.1176	0.22018	19.0	19.1	+9.3	-7.8
7	37.1812	0.22027	19.0	19.1	+9.6	-11.1
8	37.2246	0.22022	19.7	19.1	+9.6	-7.5
9	37.2499	0.22031	19.1	19.1	+9.3	-11.7
10	37.2920	0.22028	19.5	19.0	+9.9	-6.9
11	37.3170	0.22035	19.2	19.3	+8.7	-8.4
12	37.3176	0.22039	19.2	19.0	+9.3	-10.8
13	37.3319	0.22035	19.3	19.4	+8.1	-10.5
14	37.3429	0.22043	19.0	19.0	+9.3	-10.5
15	37.3452	0.22040	19.0	19.1	+9.3	-8.4
16	37.3472	0.22038	19.1	19.4	+8.1	-10.8
17	37.3519	0.22043	19.0	19.1	+9.0	-10.2
18	37.3551	0.22040	19.0	19.4	+8.1	-10.8
19	37.3860	0.22044	19.2	19.0	+9.0	-11.7
20	37.4583	0.22044	19.7	19.2	+8.1	-9.6

The total generation number is also influenced by the ideal and aspiration levels and the initial population size of genomes, but in the averaged sense it was within the range between 110 and 140. The penalty parameter r_p is set by 1.0 and the ideal levels for the peak strain energy and the cornering coefficient which were determined by the single-objective optimization using genetic algorithm were 30.605 and 0.2208 respectively. In order to obtain a Pareto curve shown in Fig. 8, the aspiration levels of two single-objective functions are adjusted simultaneously in the opposite direction to each other; from the ideal level to the current value for the peak strain energy and vice versa for the cornering coefficient.

Referring to Fig. 8, the peak strain energy and the cornering coefficient of the current design model are 38.50 and 0.22, and there is no Pareto solution better than the current design model within the predefined range of design variables. The detailed numerical values of the optimum design variables and the single-objective functions for 16 different adjustment cases of the aspiration levels are given in Table A2 in appendix. It is observed that the cornering coefficient improves as the belt angle and width become smaller and vice versa for the peak strain energy, showing the apparent reverse trend of two single-objective functions to each other to the change of design variables. Referring to Fig. 9, the two belt angles are lower-bounded when the peak strain

energy is greater than 30.7 and 35.3 respectively, while the two belt widths are upper-bounded when the peak strain energy is lower than 35.3 and 30.9 respectively. Referring to the tire structure shown in Fig. 1(a), the lateral bending stiffness of tire increases in proportional to the belt width and belt angle, so the resulting lateral bending deformation and the peak strain energy become smaller.

In order to obtain a Pareto curve better than one shown in Fig. 9, the range of design variables is extended by changing the preset constraints to $19^\circ \leq X_1 \leq 29^\circ$ and $-15 \text{ mm} \leq X_2 \leq +15 \text{ mm}$. According to the extension of the design variable range, the case numbers of each design variable increase to $N_1^{case} = N_2^{case} = 101$ and $N_3^{case} = N_4^{case} = 301$, requiring 27 bits to express each design variable vector X using a binary string. The previously approximated artificial neural networks and the previous ideal levels chosen for the peak strain energy and the cornering coefficient are used without change, as well as the simulation parameters taken for the MOGA optimization are kept unchanged.

It is observed from Fig. 10 that the Pareto curve moves towards the ideal level and its upper part is better than the current design model. Thus, one can choose a Pareto solution providing the peak strain energy and cornering coefficient better than those of the current design model. The detailed numerical values of the optimum design variables and the corresponding single-objective functions in the upper Pareto region are recorded in Table 1. When restricted to the upper Pareto region, it can be observed from the comparison with the values in Table A1 that the angles of belt #1 and #2 increase from 19° to 21° , while the width of belt #1 becomes larger and vice versa for belt #2.

5. Conclusions

The multi-objective optimum design of the belt composite structure automobile tire was carried out, in which the continuous design variables were discretized into a number of discrete ones and each discrete tire structure model was coded into a binary string. In order to rule out the possibility of any pre-matured Pareto solution, the genetic evolution was forced to iterate up to the preset minimum generation number without the fitness test at the initial stages. And, the convergence of the genetic evolution was judged by the preset maximum repetition times of successive generations with the best fitness unchanged.

Through the numerical experiments, it has been verified that the proposed MOGA optimization algorithm successfully seeks the Pareto solutions for all the combinations of aspiration levels. Even though the numerical experiments dealt in this paper are restricted to the tire reinforcement structure and the aspiration levels are adjusted by rather uniformly, it is convinced that the presented MOGA optimization method can successfully provide one a best Pareto solution for any kind of discrete-type multi-objective optimization problem in various engineering applications.

Acknowledgements

The financial support given to one of authors (S.B. Lee) for this work by Pusan National University under the independent academic research fund (two years) is gratefully acknowledged.

References

- Abe, A., Kamegawa, T. and Nakajima, Y. (1996), "Optimum young's modulus distributions in tire design", *Tire Sci. Technol.*, **24**(3), 204-219.
- Abe, A., Kamegawa, T. and Nakajima, Y. (2004), "Optimization of construction of tire reinforcement by genetic algorithm", *Optim. Eng.*, **5**(1), 77-92.
- Bathe, K.J. (1996), *Finite Element Procedures*, Prentice-Hall, New Jersey.
- Brunskill, A. and Lubitz, W.D. (2012), "A neural network shelter model for small wind turbine siting near single obstacles", *Wind Struct. Int. J.*, **15**(1), 43-64.
- Cho, C.S., Choi, E.H., Cho, J.R. and Lim, O.K. (2011), "Topology and parameter optimization of a foaming jig reinforcement structure by the response surface method", *Comput. Aided Des.*, **43**(12), 1707-1716.
- Cho, J.R. and Park, H.J. (2003), "Effective volume-fraction optimization for thermal stress reduction in FGMs using irregular h-refinement", *Int. J. Numer. Meth. Eng.*, **58**(5), 749-770.
- Cho, J.R., Jeong, H.S. and Yoo, W.S. (2002), "Multi-objective optimization of tire carcass contours using a systematic aspiration-level adjustment procedure", *Comput. Mech.*, **29**(6), 498-509.
- Cho, J.R., Shin, S.W. and Yoo, W.S. (2005), "Crown shape optimization for enhancing the tire wear performance by ANN", *Comput. Struct.*, **83**(12-13), 920-933.
- Clark, S.K. (1982), *Mechanics of Pneumatic Tires*, Government Printing Office, Washington D.C.
- Danielson, K.T., Noor, A.K. and Green, J.S. (1996), "Computational strategies for tire modeling and analysis", *Comput. Struct.*, **61**(4), 673-693.
- Demkowicz, L., Oden, J.T., Rachowicz, W. and Hardy, D. (1989), "Toward a universal *h-p* adaptive finite element strategy, Part 1: Constrained approximation and data structure", *Comput. Method. App. Mech. Eng.*, **77**(1-2), 79-112.
- Gao, H.Y., Guo, X.L. and Hu, X.F. (2012), "Crack identification based on Kriging surrogate model", *Struct. Eng. Mech. Int. J.*, **41**(1), 25-41.
- Goldberg, D.E. (1989), *Genetic Algorithms in Search, Optimization & Machine Learning*, Addison-Wesley.
- Govindaraj, V. and Ramasamy, J.V. (2005), "Optimum detailed design of reinforced concrete continuous beams using genetic algorithms", *Comput. Struct.*, **84**(1-2), 34-48.
- Hibbit, Karlsson & Sorensen Inc. (2007), *ABAQUS/Standard User's Manual*, Ver. 6.7, Pawtucket.
- Hoffmeister, K. and Bernard, J. (1998), "Tread pitch arrangement optimization through the use of a genetic algorithm", *Tire Sci. Technol.*, **26**(1), 2-22.
- Holland, J.H. (1975), *Adaptation on Natural and Artificial Systems*, The University of Michigan Press, Ann Arbor.
- Huang, X. and Xie, Y.M. (2009), "Bi-directional evolutionary topology optimization of continuum structures with one or multiple materials", *Comput. Mech.*, **43**(3), 393-401.
- Kameshki, E.S. and Saka, M.P. (2007), "Optimum design of nonlinear braced domes using genetic algorithm", *Comput. Struct.*, **85**(1-2), 71-79.
- Lindtner, E.K. and Tseng, N.T. (1992), "Finite element analysis of tread pattern model", *Proceedings of Eleventh Annual Meeting Tire Society Conference*, Akron, Ohio.
- Meschke, G., Payer, H.J. and Mang, H.A. (1995), "3D simulations of automobile tires: material modeling, mesh generation, and solution strategies", *Tire Sci. Technol.*, **25**(3), 175-188.
- Nakajima, Y., Kadowaki, H., Kamegawa, T. and Ueno, K. (1992), "Application of a neural network for the optimization of tire design", *Tire Sci. Technol.*, **27**(2), 62-83.
- Nakajima, Y., Kamegawa, T. and Abe, A. (1996), "Theory of optimum tire contour and its application," *Tire Sci. Technol.*, **24**(3), 184-203.
- Nakayama, H. and Furukawa, K. (1985), "Satisficing trade-off method with an application to multiobjective structural design", *Large Scale Syst.*, **8**, 47-57.
- Purdy, J.F. (1963), *Mathematics Underlying Design of Pneumatic Tires*, Edwards Brothers, Ann Arbor.
- Rahami, H., Kaveh, A. and Gholipour, Y. (2008), "Sizing, geometry and topology optimization of trusses via force method and genetic algorithm", *Eng. Struct.*, **30**(9), 2360-2369.
- Sarker, R., Mohammadian, M. and Yao, X. (2002), *Evolutionary Optimization*, Kluwer Academic Publishers

- Group, Massachusetts.
- Satyamurthy, K. and Hirschfeld, L.R. (1987), "An axisymmetric finite element and its use to examine the effects of construction variables on radial tire", *Tire Sci. Technol.*, **15**(2), 97-122.
- Shiraishi, M., Yishinaga, H. and Miyori, A. (2000), "Simulation of dynamically rolling tire", *Tire Sci. Technol.*, **28**(4), 264-276.
- Simpson, P.K. (1991), *Artificial Neural Systems*, Pergamon Press, New York.
- Smith, O.D. and Holland, J. (1987), "A study of permutation crossover operators on the traveling salesman problem", *Proceedings of International Conference Genetic Algorithms*, 224-230.

CC

Appendix A: Material properties and optimization results

Table A1 Structural composition and material properties of fiber-reinforced composite parts

Item	Components		
	Carcass	Belt	Capply
Number	1	2	2
Angle (°)	+ 90	variable (21~27)	0/0
EPI	26	16	30
Modulus (psi)	0.478×10^6	0.182×10^8	0.230×10^5

Table A2 Multi-objective optimization results of fiber-reinforced belt layer (PSS: peak strain energy, CC: cornering coefficient)

Aspiration level adjustment	Objective functions		Optimum design variables			
			Belt angles (deg)		Width increments (mm)	
	PSS (psi)	CC	#1	#2	#1	#2
1	30.6116	0.2055	21.9	25.0	+ 10.0	+ 10.0
2	30.7287	0.2065	21.0	25.1	+ 10.0	+ 10.0
3	30.9679	0.2075	21.0	24.5	+ 9.8	+ 9.8
4	31.2580	0.2085	21.0	23.9	+ 10.0	+ 10.0
5	31.6044	0.2095	21.0	23.6	+ 10.0	+ 8.8
6	31.9762	0.2105	21.0	23.4	+ 9.8	+ 7.2
7	32.3379	0.2115	21.0	23.1	+ 10.0	+ 5.8
8	32.7265	0.2125	21.0	22.8	+ 10.0	+ 4.6
9	33.1302	0.2135	21.0	22.5	+ 10.0	+ 3.2
10	33.5762	0.2145	21.0	22.2	+ 10.0	+ 1.0
11	34.0509	0.2155	21.0	21.8	+ 10.0	- 0.4
12	34.6086	0.2165	21.0	21.3	+ 10.0	- 0.4
13	35.3283	0.2175	21.0	21.0	+ 9.0	- 3.0
14	36.2491	0.2185	21.0	21.0	+ 6.6	- 4.4
15	37.6152	0.2195	21.0	21.0	+ 3.4	- 5.8
16	40.4787	0.2205	21.0	21.0	- 0.8	- 5.2

List of symbols

X	Design variable vector
X_I	I -th distinct design variable vector
$f_i(X)$	Individual single-objective functions
nd, no	Numbers of design variables and single-objective functions
ng	Number of distinct design variable vectors
$F(X)$	Multi-objective function
$g_j(X)$	j -th constraint
f_i^*	Ideal level for the i -th single-objective function
\hat{f}_i	Aspiration level for the i -th single-objective function
$F^k(X)$	Weighted multi-objective function at the k -th trade-off stage
w_i^k	Weighting factor for the i -th single-objective function
$U^k(X, r_p)$	Unconstrained multi-objective function at the k -th trade-off stage
r_p, c_j^k	Penalty parameter and scaling factor for the j -th constraint
N_{pop}, m_{nd}	Population size and the binary string size
G_{ID}	ID -th genome (design model) in the population
N_{TOT}^{case}	Total case number of design variable vector X
N_i^{case}	Case number of the i -th design variable X_i
\mathcal{G}_G^0	Initial population of genomes
$U^{k,\ell}$	Fitness value of the i -th genome at the ℓ -th genetic evolution
N_{GA}^{con}	Maximum repetition times of successive generations with the best fitness unchanged
N_{GA}^{for}	Minimum forced generation number
f_i^{TAR}	Target output data for the i -th single-objective functions f_i
f_i^{INP}	Input data for single-objective function f_i
f_i^{OUT}	Output signal of the i -th single-objective function from ANN
w_{ij}	Weighting factors for ANN
\mathcal{E}_{ANN}	Convergence tolerance for determining the weighting weights w_{ij}
N_{DOE}	Number of experiments in DOE